LAWRENCE
LIVERMORE
NATIONAL
LABORATORY

LLNL-TR-852480

M4SF-23LL010302052-Radionuclide Interaction with Hydrothermally Altered Repository Materials

E. Balboni, L. Williams, F. Caporuscio, A. Zandanel, M. Mills, Y. Wang, M. Zavarin, S. Han

July 31, 2023

Disclaimer

This work performed under the auspices of the U.S. Department of Energy by Lawrence Livermore National Laboratory under Contract DE-AC52-07NA27344.

July 21, 2023

M4SF-23LL010302052-Radionuclide Interaction with Hydrothermally Altered Repository Materials

E. Balboni[1], Liuba Williams[1], Florie Caporuscio[2], Amber Elizabeth Zandanel[2], Melissa Mills[3], Yifeng Wang[3], M. Zavarin[1], S. Han[1]

[1] Glenn T. Seaborg Institute, Physical & Life Sciences, Lawrence Livermore National Laboratory, 7000 East Avenue, Livermore, CA 94550 USA.
[2] Los Alamos National Laboratory, Los Alamos, NM USA
[3] Sandia National Laboratory, Albuquerque, NM USA

DISCLAIMER

Contents

1. Introduction 1
2. Effects of bentonite heating on radionuclides adsorption 1
2.1 Materials and Methods 2
2.2 Results 4
2.3 Outlook and Future Work 6
3. A Comprehensive Surface Complexation Reaction Analysis Workflow: Surface complexation of Se(IV) and Se(VI) on Iron Oxide Phases 7
3.1 Development of Radionuclide Surface Complexation Modeling Framework 7
3.2 Case Study of Selenium Sorption to Ferrihydrite 8
3.3 Outlook and Future Work 13
4. FY24 Planned Efforts 13
5. Acknowledgments 14
6. References 14

1. Introduction

This progress report (Level 4 Milestone Number M4SF-23LL010302052) summarizes research conducted at Lawrence Livermore National Laboratory (LLNL) within the Crystalline Activity Number SF-23LL01030205. The research is focused on actinide and radionuclide sequestration in hydrothermally altered repository materials.

In FY23, a manuscript was in preparation for publication summarizing our analysis of radionuclide sorption and coprecipitation into Fe oxide phases and evaluation of radionuclide partitioning values across a range of radionuclides relevant to performance assessment. We demonstrated our approach in detail using Se sorption and coprecipitation with iron oxide minerals. These data were presented in our FY22 annual report and will not be repeated here.

We also initiated experiments to identify radionuclide interaction with hydrothermally altered crystalline repository and backfill materials. Recent research performed at Los Alamos National Laboratory (LANL) and Sandia National Laboratory (SNL) has provided key insights regarding the hydrothermal alteration behavior of bentonite backfill in the presence of repository materials (steel, concrete, etc.). We are now examining how mineral alteration affects retardation behavior of plutonium and a suite of other radionuclides. These experiments also allow us to test the predictive ability of our component additivity approach to surface complexation and ion exchange. Our guiding hypothesis is that a robust surface complexation/ion exchange model and associated database, developed using our L-SCIE approach, can effectively predict changes in radionuclide sorption behavior resulting from the hydrothermal alteration of mineralogy in a repository near field. A short update of results to date is presented below.

A manuscript was also in preparation describing a self-consistent model and approach to simulating Se(IV) and Se(VI) sorption to 5 iron oxide phases based on our L-SCIE community database. This will be the first implementation of a multi-mineral and multi-oxidation state sorption model using our new L-SCIE database and workflow. A short summary of these results is presented below.

2. Effects of bentonite heating on radionuclides adsorption

One of the more accepted ideas for high-level nuclear waste disposal is to emplace steel waste canisters in a geological repository with a bentonite/clay barrier between the canister and host rock (Meunier et al., 1998; Pusch, 1979). Bentonite is used to provide 1) a physical barrier to prevent fluid seeping in from natural surroundings and interacting with the waste package and 2) a chemical barrier by attenuating actinide migration if a release occurs.

High temperatures (100–200 °C) near waste canisters resulting from radioactive decay may alter the bentonite clay's ability to adsorb contaminants. Temperature effects on the bentonite/clay barrier may include changes to the clay's hydrological and mechanical properties, changes to pore water chemical compositions, and changes to the clay and

accessory mineral composition (Cuadros and Linares, 1996; Wersin et al., 2007; Zheng et al., 2017). For these reasons the effects of elevated temperature on the engineered barrier must be taken into account when designing a nuclear waste repository

In this study, we examine the capacity of hydrothermally altered clay samples (Table 1) to adsorb radionuclides (Table 2) in batch sorption experiments. The hydrothermally altered samples were subjected to short-term (days to months)- high temperature (200-300 °C) heating in the laboratory.

2.1 Materials and Methods

The hydrothermally altered samples used in this study were provided by collaborators from LANL and SNL (Table 1). All the samples received at LLNL were prepared for surface area analysis using BET, but no further characterization was performed at LLNL as complete chemical and mineralogical characterization of the selected samples was presented in previous publications (Caporuscio, 2014, 2015; Caporuscio, 2018; Caporuscio, 2019; Caporuscio, 2020; Cheshire et al., 2014; Mills et al., 2023).

In this work, batch sorption experiments with hydrothermally altered clays (Table 1) and different radionuclides (Table 2) are performed at a pH range of 7-8 using either a low (NaCl 0.01M, $NaHCO_3$ 0.01M) or high (NaCl 1M, $NaHCO_3$ 0.01M) ionic strength buffer solution as background electrolyte. In both low and high ionic strength solutions, a 0.01M HEPES buffer is used to maintain the pH in the desired range. Each sorption experiment is performed in triplicate using a solid to solution ratio of 5 g/L. To monitor the effects of heating on the adsorption properties of bentonite, batch sorption experiments are also performed using control (unheated) bentonite samples (Table 1). A list of all the radionuclides and the materials used for sorption experiments is reported in Table 1 and Table 2.

Table 1. List of samples used for sorption experiments. Samples (unheated and hydrothermally altered) were provided by collaborators at Los Alamos National Laboratory (LANL) and Sandia National Laboratory (SNL). Cation exchange of selected unheated samples was performed at SNL (K, Na) and Lawrence Livermore National Laboratory (LLNL).

Mineralogical composition	Sample origin	Sample Name			
Unheated samples					
Wyoming Bentonite	LANL	**WY**			
Opalinus Clay	LANL	**OPC**			
Grimsel Granodiorite	LANL	**GG**			
Illite	SNL	**IMt-1**			
Illite/Smectite (70:30) mixed layers	SNL	**ISCz-1**			
Cation exchanged unheated samples			**Cation Exchange Solution**		
Na-exchanged Wyoming Bentonite	LANL/ LLNL	**Na-WY**	1M $NaC_2H_3O_2$		
Na-exchanged Opalinus Clay	LANL/ LLNL	**Na-OPC**	1M $NaC_2H_3O_2$		
K-exchanged Smectite	SNL	**K-Swy-2-SNL**	1M KCl		
Na-exchanged Wyoming bentonite	SNL	**Na-SWy-2-SNL**	1M NaCl		
Hydrothermally altered samples			**Hydrothermal Alteration Conditions**		
			Synthetic Ground Water Type	**Temperature (C)**	**Duration of Hydrothermal Experiment**
Wyoming Bentonite and 304 SS	LANL	**EBS-5**	Stripa V2.1	300	6 weeks
Wyoming Bentonite and Quartz Sand	LANL	**EBS-9**	Stripa V2.2	25/100/200/300/25	5 weeks
Wyoming Bentonite and 316 SS	LANL	**EBS-10**	Stripa V2.3	300	6 weeks
Wyoming Bentonite	LANL	**EBS-12**	Stripa V2.3	300	7 weeks
Wyoming Bentonite, Opalinus Clay, and 316 SS	LANL	**EBS-15**	Synthetic Opalinus GW	300	6 weeks
Wyoming Bentonite, Opalinus Clay, and 304 SS	LANL	**EBS-19**	Synthetic Opalinus GW	300	6 weeks
Wyoming Bentonite, Opalinus Clay, and 316 SS	LANL	**EBS-20**	Synthetic Opalinus GW	300	6 months
Wyoming Bentonite, Opalinus Clay, and Portland Cement	LANL	**EBS-28**	Synthetic Opalinus GW	300	8 weeks
Wyoming Bentonite, Grimsel Granodiorite, and 316 SS	LANL	**IEBS-5**	Synthetic Grimsel GW	250	8 weeks
Wyoming Bentonite, Grimsel Granodiorite, and Portland Cement	LANL	**IEBS-6**	Synthetic Grimsel GW	250	8 weeks
K exchanged Wyoming bentonite	SNL	**K-1000**	1M KCl	200	28 days

Table 2. List of radionuclides chosen for adsorption studies with hydrothermally altered samples. The column labeled FY indicates the status of the work and/or when it will be completed.

Radionuclide	Oxidation state	FY
^{137}Cs	(I)	2023 (complete, data analysis in progress)
^{90}Sr	(II)	2023 (start)
^{243}Am	(III)	2023 (complete)
^{238}Pu	(IV)	2024
^{237}Np	(V)	2024
^{233}U	(VI)	2024
^{99}Tc	(VII)	2024

2.2 Results

In FY23, we completed and analyzed data for the ^{137}Cs sorption experiments using samples provided by LANL. Batch sorption experiments using the hydrothermally altered samples provided by SNL are currently underway and will be completed by the end of FY23.

Figure 1 reports the ^{137}Cs partition coefficient (Kd, mL/g) calculated for unheated samples (OPC, Wy, GG, Na-Wy. Bent, Na-OPC) and hydrothermally altered samples (EBS 5, EBS9, EBS 10, EBS 12, EBS 15, EBS 19, EBS20, EBS28, IEBS5 and IEBS 6) in low ionic strength buffer solutions. For the unheated samples, the calculated Kd values range between 250-440 mL/g, with the Na- exchanged forms of OC and WY displaying slightly higher Kd values compared to their non-exchanged forms. As expected, the Grimsel granodiorite sample (GG) has the lowest measured Kd value (~10 mL/g). The Kd values calculated for the majority of the hydrothermally altered samples are within expected Kd ranges of unheated Opalinus clay and Wyoming bentonite (Wy, Na-Wy, OPC, Na-OPC), however samples EBS 12 and EBS 28 display lower Kd values (< 250 mL/g) (Figure 1, red line, red arrows).

In experiments conducted using a high ionic strength background electrolyte, the Kd values for the unheated samples range between 40-170 mL/g, with the Na- exchanged forms of OC and WY displaying lower Kd values compared to their non-exchanged forms. All of the Kd values calculated for sorption experiments conducted at high ionic strength are lower than Kd values calculated for experiments conducted at low ionic strength (Figure 2), consistent with a Cs sorption behavior that is dominated by an ion exchange mechanism. Samples EBS 12 and EBS 28 display lower Kd values compared to unheated samples, consistent with the low ionic strength experiments. Additionally, samples EBS 9, IEBS 5 and IEBS 6 also display decreased sorption capacity in high ionic strength background electrolyte (Kd < 40 mL/g) (Figure 2, red line, red arrows). All batch sorption experiments were performed in triplicate and results display good reproducibility (Figures 1 and 2).

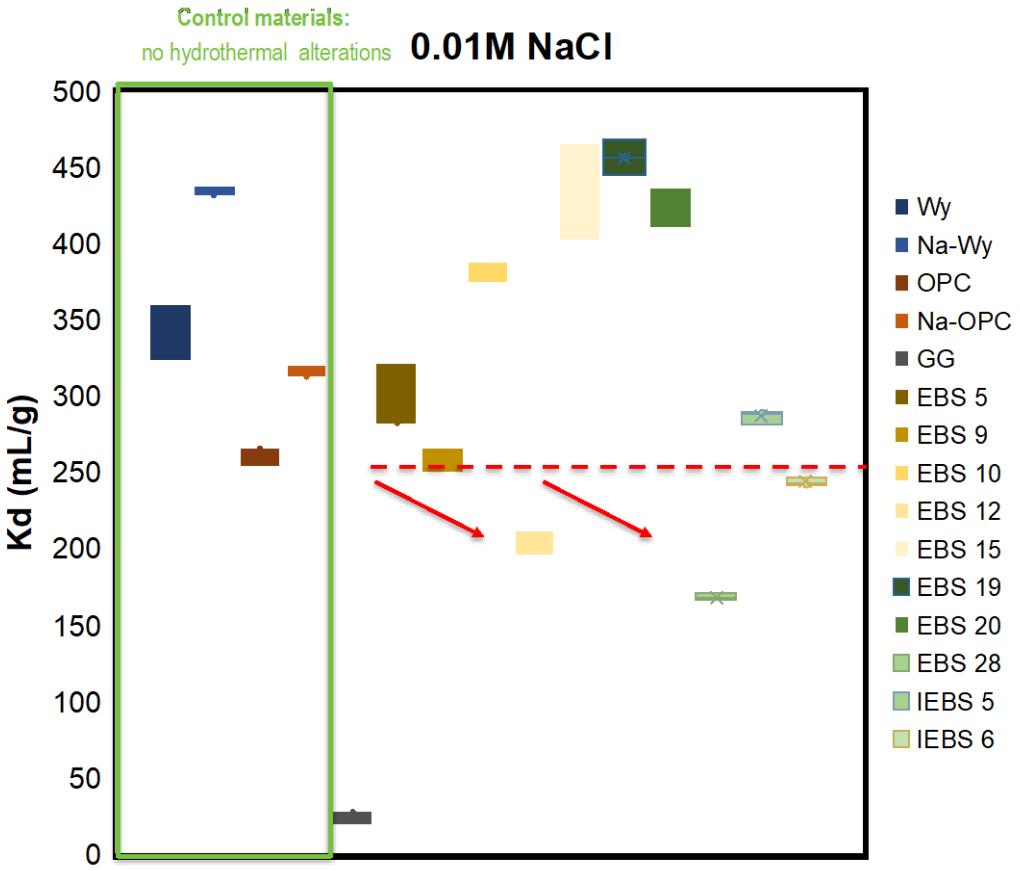

Figure 1. Values of Kd (mL/g) calculated for ^{137}Cs batch sorption experiments using hydrothermally altered samples (EBS5, EBS9, EBS10, EBS12,EBS15, EBS19, EBS20, EBS28, IEBS5 and IEBS6) and unheated samples (green box: Wy, Na-Wy, OPC, Na-OPC, GG) in low ionic strength background electrolyte (0.011M NaCl, 0.01M $NaHCO_3$, 0.01M HEPES). Each experiment was performed in triplicates.

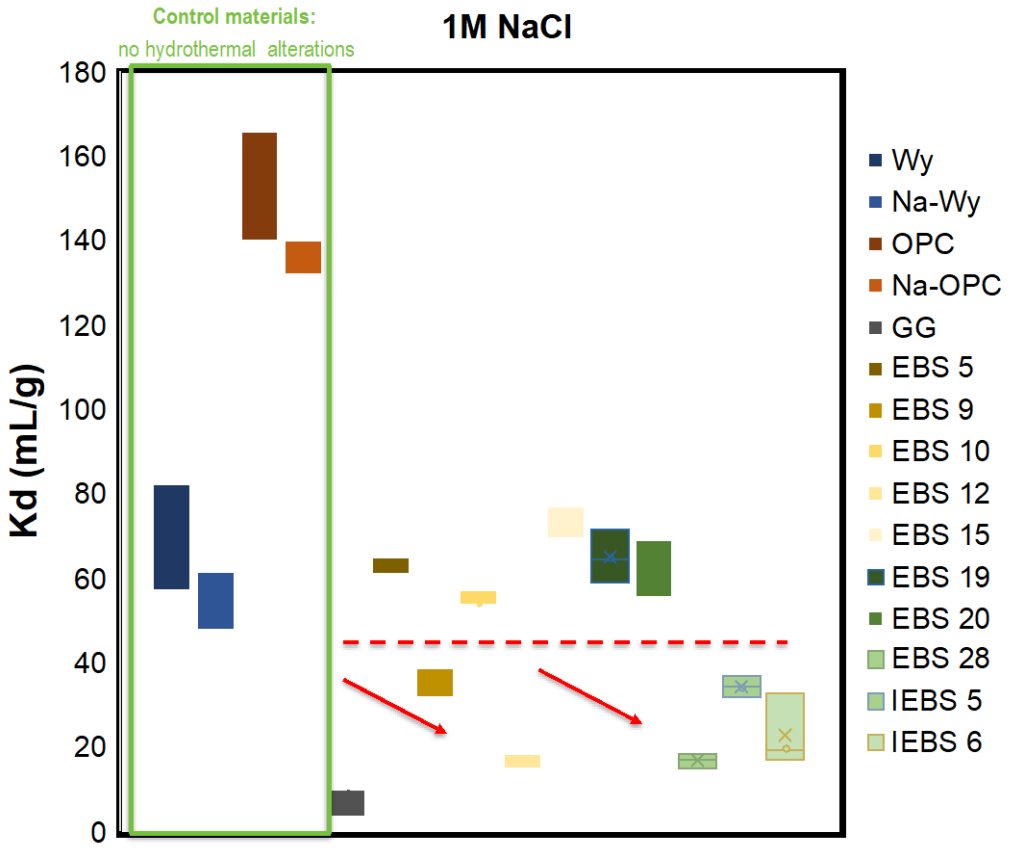

Figure 2. Values of Kd (mL/g) calculated for ^{137}Cs batch sorption experiments using hydrothermally altered samples (EBS5, EBS9, EBS10, EBS12,EBS15, EBS19, EBS20, EBS28, IEBS5 and IEBS6) and unheated samples (green box: Wy, Na-Wy, OPC, Na-OPC, GG) in high ionic strength background electrolyte (1M NaCl, 0.01M $NaHCO_3$, 0.01M HEPES). Each experiment was performed in triplicates.

2.3 Outlook and Future Work

Observed changes in radionuclide adsorption after bentonite/clay heating have implications for radionuclide diffusive transport through engineered barriers and must be considered when designing waste disposal repositories. Results from this comprehensive analysis will inform performance assessment models on how much reduction of Kd values can be expected for the original clay material as a result of heating under different ionic strengths.

Sorption experiments and data analysis for ^{137}Cs and for ^{243}Am will be completed by the end of FY23. These experiments are currently underway and are part Liuba Williams' (UNLV) summer internship project at LLNL. In FY24 we will complete the study including all other radionuclides reported in Table 1 and perform a modeling analysis to identify processes and mechanisms driving the observed changes in radionuclide sorption behavior.

3. A Comprehensive Surface Complexation Reaction Analysis Workflow: Surface complexation of Se(IV) and Se(VI) on Iron Oxide Phases

3.1 Development of Radionuclide Surface Complexation Modeling Framework

Surface complexation models (SCM), which address the quantification of sorption processes, play a key role in Geological Disposal Safety Assessment (GDSA). Although enormous amounts of efforts have been made to develop reliable SCMs, obtaining global consensus among reported SCMs is still challenging since each SCM had been constructed with different foundations. In light of the limitation, this task aims at developing a more comprehensive SCM framework by compiling raw sorption data and the relevant surface complexation reactions reported from various literature sources. This effort is a follow-on to the earlier study supported by the crystalline work package that examined the sorption and coprecipitation of Se with iron(II) and iron(III) oxide mineral phases and reported in the FY22 milestone report.

Figure 3 describes the framework for SCM database development. The framework consists of a sorption database, i.e., L-SCIE (LLNL Surface Complexation/Ion Exchange) (Zavarin et al., 2022), a surface titration model, and a surface complexation model. L-SCIE database provides input data for surface titration/complexation models, and data processing and fitting routine have been done within each model.

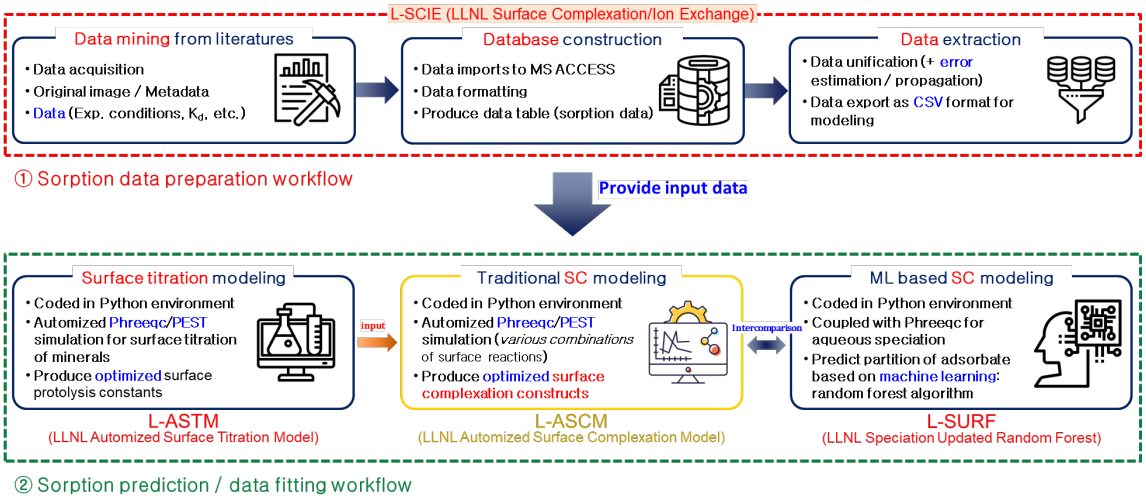

Figure 3. Workflow of community data driven surface complexation modeling framework

The newly developed SCM, LLNL Automized Surface Complexation Model (L-ASCM), was written in Python and the code was integrated with PhreeqC (Parkhurst and Appelo,

2013) and PEST (Doherty, 2018) for data fitting. One of the key features of the current model is that the model enables automation of the entire modeling process, for example, pre data analysis, input file generation, execution of data fitting routine, post simulation analysis, and visualization of simulation results. Furthermore, the model automatically examines the fitting for all possible SCM structural configurations (e.g., types of SCM and surface reactions) without any user interference.

The details of the workflow of L-ASTM are shown in Figure 4. First, the code imports sorption data extracted from the L-SCIE database. Like an example of Se(IV)-ferrihydrite sorption system given in Table 3, there could be a number of surface complexation reactions for given mineral and adsorbate pair from different literature references. The L-ASCM makes a list of all possible surface complexation reaction combinations and produces the relevant SCM constructs for all combinations. Then the code generates the PHREEQC/PEST input files for each SCM construct and runs simulations for all possible SCM constructs. Once the simulations are done, the code automatically evaluates the quality of each SCM construct and finally, the optimized SCM constructs with the relevant surface complexation reactions and the corresponding reaction constants are produced.

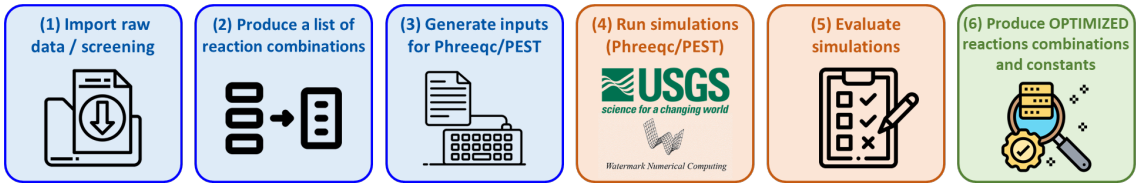

Figure 4. Surface complexation modeling workflow (L-ASCM code) for adsorption data.

Table 3. Surface complexation reactions of selenium sorption to ferrihydrite as reported in the RES^{3}T database (Brendler et al., 2003; Dresden-Rossendorf, 2013).

	Surface complexation reactions	Initial $\log_{10}K$	Reference
1	$\text{»Fe-OH} + SeO_3^{2-} \leftrightarrow \text{»Fe-OH-}SeO_3^{2-}$	5.17	(Dzombak and Morel, 1990)
2	$\text{»Fe-OH} + SeO_3^{2-} + H^+ \leftrightarrow \text{»Fe-OH}_2\text{-}SeO_3^-$	12.90	(Benjamin and Bloom, 1981)
3	$\text{»Fe-OH} + SeO_3^{2-} + 2H^+ \leftrightarrow \text{»Fe-OH}_2\text{-}HSeO_3$	22.00	(Benjamin and Bloom, 1981)
4	$\text{»Fe-OH} + SeO_3^{2-} + 3H^+ \leftrightarrow \text{»Fe-OH}_2\text{-}SeO_3H_2^+$	29.00[a]	-*
5	$2\text{»Fe-OH} + SeO_3^{2-} \leftrightarrow (\text{»Fe-O})_2\text{-}SeO_3^{4-} + 2H^+$	-6.96	(Wang et al., 2001)
6	$2\text{»Fe-OH} + SeO_3^{2-} + 2H^+ \leftrightarrow (\text{»Fe-OH}_2)_2\text{-}SeO_3$	26.06	(Wang et al., 2001)

[a]Presumed value. *Newly added in this work

3.2 Case Study of Selenium Sorption to Ferrihydrite

Sorption characteristics of selenium to ferrihydrite were examined using L-ASCM and community selenium sorption data. For Se(IV) – ferrihydrite sorption system, six surface

complexation reactions (Table 3) and the diffuse double layer model (DDLM) were employed. Since six surface complexation reactions were used, a total of 63 reaction combinations were obtained (Table 4). In other words, 63 different SCM constructs had been tested to find appropriate surface complexation reactions which can model Se(IV) sorption to ferrihydrite. The quality of each SCM construct was evaluated based on weighted Pearson correlation coefficient (R value) and standard deviation (SD) of surface complexation reaction constant calculated from the model. If the R value is higher than 0.9 and SDs of all reaction constants are lower than 1.0, it was presumed that the model has a good quality.

Table 4. List of surface complexation reaction combinations: Se(IV) – ferrihydrite sorption system.

SCM construct	Surface species	SCM construct	Surface species
	One species reaction	**33**	»Fe-OH_2-SeO_3^-, »Fe-OH_2-$HSeO_3$, (»Fe-O)$_2$-SeO_3^{4-}
1	»Fe-OH-SeO_3^{2-}	**34**	»Fe-OH_2-SeO_3^-, »Fe-OH_2-$HSeO_3$, (»Fe-OH_2)$_2$-SeO_3
2	»Fe-OH_2-SeO_3^-	**35**	»Fe-OH_2-SeO_3^-, »Fe-OH_2-$SeO_3H_2^+$, (»Fe-O)$_2$-SeO_3^{4-}
3	»Fe-OH_2-$HSeO_3$	**36**	»Fe-OH_2-SeO_3^-, »Fe-OH_2-$SeO_3H_2^+$, (»Fe-OH_2)$_2$-SeO_3
4	»Fe-OH_2-$SeO_3H_2^+$	**37**	»Fe-OH_2-SeO_3^-, (»Fe-O)$_2$-SeO_3^{4-}, (»Fe-OH_2)$_2$-SeO_3
5	(»Fe-O)$_2$-SeO_3^{4-}	**38**	»Fe-OH_2-$HSeO_3$, »Fe-OH_2-$SeO_3H_2^+$, (»Fe-O)$_2$-SeO_3^{4-}
6	(»Fe-OH_2)$_2$-SeO_3	**39**	»Fe-OH_2-$HSeO_3$, »Fe-OH_2-$SeO_3H_2^+$, (»Fe-OH_2)$_2$-SeO_3
	Two species reaction	**40**	»Fe-OH_2-$HSeO_3$, (»Fe-O)$_2$-SeO_3^{4-}, (»Fe-OH_2)$_2$-SeO_3
7	»Fe-OH-SeO_3^{2-}, »Fe-OH_2-SeO_3^-	**41**	»Fe-OH_2-$SeO_3H_2^+$, (»Fe-O)$_2$-SeO_3^{4-}, (»Fe-OH_2)$_2$-SeO_3
8	»Fe-OH-SeO_3^{2-}, »Fe-OH_2-$HSeO_3$		**Four species reaction**
9	»Fe-OH-SeO_3^{2-}, »Fe-OH_2-$SeO_3H_2^+$	**42**	»Fe-OH-SeO_3^{2-}, »Fe-OH_2-SeO_3^-, »Fe-OH_2-$HSeO_3$, »Fe-OH_2-$SeO_3H_2^+$
10	»Fe-OH-SeO_3^{2-}, (»Fe-O)$_2$-SeO_3^{4-}	**43**	»Fe-OH-SeO_3^{2-}, »Fe-OH_2-SeO_3^-, »Fe-OH_2-$HSeO_3$, (»Fe-O)$_2$-SeO_3^{4-}
11	»Fe-OH-SeO_3^{2-}, (»Fe-OH_2)$_2$-SeO_3	**44**	»Fe-OH-SeO_3^{2-}, »Fe-OH_2-SeO_3^-, »Fe-OH_2-$HSeO_3$, (»Fe-OH_2)$_2$-SeO_3
12	»Fe-OH_2-SeO_3^-, »Fe-OH_2-$HSeO_3$	**45**	»Fe-OH-SeO_3^{2-}, »Fe-OH_2-SeO_3^-, »Fe-OH_2-$SeO_3H_2^+$, (»Fe-O)$_2$-SeO_3^{4-}
13	»Fe-OH_2-SeO_3^-, »Fe-OH_2-$SeO_3H_2^+$	**46**	»Fe-OH-SeO_3^{2-}, »Fe-OH_2-SeO_3^-, »Fe-OH_2-$SeO_3H_2^+$, (»Fe-OH_2)$_2$-SeO_3
14	»Fe-OH_2-SeO_3^-, (»Fe-O)$_2$-SeO_3^{4-}	**47**	»Fe-OH-SeO_3^{2-}, »Fe-OH_2-SeO_3^-, (»Fe-O)$_2$-SeO_3^{4-}, (»Fe-OH_2)$_2$-SeO_3
15	»Fe-OH_2-SeO_3^-, (»Fe-OH_2)$_2$-SeO_3	**48**	»Fe-OH-SeO_3^{2-}, »Fe-OH_2-$HSeO_3$, »Fe-OH_2-$SeO_3H_2^+$, (»Fe-O)$_2$-SeO_3^{4-}
16	»Fe-OH_2-$HSeO_3$, »Fe-OH_2-$SeO_3H_2^+$	**49**	»Fe-OH-SeO_3^{2-}, »Fe-OH_2-$HSeO_3$, »Fe-OH_2-$SeO_3H_2^+$, (»Fe-OH_2)$_2$-SeO_3
17	»Fe-OH_2-$HSeO_3$, (»Fe-O)$_2$-SeO_3^{4-}	**50**	»Fe-OH-SeO_3^{2-}, »Fe-OH_2-$HSeO_3$, (»Fe-O)$_2$-SeO_3^{4-}, (»Fe-OH_2)$_2$-SeO_3

SCM construct	Surface species	SCM construct	Surface species
18	»Fe-OH_2-$HSeO_3$, (»Fe-OH_2)$_2$-SeO_3	**51**	»Fe-OH-SeO_3^{2-}, »Fe-OH_2-$SeO_3H_2^+$ (»Fe-O)$_2$-SeO_3^{4-}, (»Fe-OH_2)$_2$-SeO_3
19	»Fe-OH_2-$SeO_3H_2^+$, (»Fe-O)$_2$-SeO_3^{4-}	**52**	»Fe-OH_2-SeO_3^-, »Fe-OH_2-$HSeO_3$, »Fe-OH_2-$SeO_3H_2^+$, (»Fe-O)$_2$-SeO_3^{4-}
20	»Fe-OH_2-$SeO_3H_2^+$, (»Fe-OH_2)$_2$-SeO_3	**53**	»Fe-OH_2-SeO_3^-, »Fe-OH_2-$HSeO_3$, »Fe-OH_2-$SeO_3H_2^+$, (»Fe-OH_2)$_2$-SeO_3
21	(»Fe-O)$_2$-SeO_3^{4-}, (»Fe-OH_2)$_2$-SeO_3	**54**	»Fe-OH_2-SeO_3^-, »Fe-OH_2-$HSeO_3$, (»Fe-O)$_2$-SeO_3^{4-}, (»Fe-OH_2)$_2$-SeO_3
	Three species reaction	**55**	»Fe-OH_2-SeO_3^-, »Fe-OH_2-$SeO_3H_2^+$, (»Fe-O)$_2$-SeO_3^{4-}, (»Fe-OH_2)$_2$-SeO_3
22	»Fe-OH-SeO_3^{2-}, »Fe-OH_2-SeO_3^-, »Fe-OH_2-$HSeO_3$		»Fe-OH_2-$HSeO_3$, »Fe-OH_2-$SeO_3H_2^+$, (»Fe-O)$_2$-SeO_3^{4-}, (»Fe-OH_2)$_2$-SeO_3
23	»Fe-OH-SeO_3^{2-}, »Fe-OH_2-SeO_3^- »Fe-OH_2-$SeO_3H_2^+$	**56**	**Five species reaction**
24	»Fe-OH-SeO_3^{2-}, »Fe-OH_2-SeO_3^- (»Fe-O)$_2$-SeO_3^{4-}	**57**	»Fe-OH-SeO_3^{2-}, »Fe-OH_2-SeO_3^-, »Fe-OH_2-$HSeO_3$, »Fe-OH_2-$SeO_3H_2^+$, (»Fe-O)$_2$-SeO_3^{4-}
25	»Fe-OH-SeO_3^{2-}, »Fe-OH_2-SeO_3^-, (»Fe-OH_2)$_2$-SeO_3	**58**	»Fe-OH-SeO_3^{2-}, »Fe-OH_2-SeO_3^-, »Fe-OH_2-$HSeO_3$, »Fe-OH_2-$SeO_3H_2^+$, (»Fe-OH_2)$_2$-SeO_3
26	»Fe-OH-SeO_3^{2-}, »Fe-OH_2-$HSeO_3$, »Fe-OH_2-$SeO_3H_2^+$	**59**	»Fe-OH-SeO_3^{2-}, »Fe-OH_2-SeO_3^-, »Fe-OH_2-$HSeO_3$, (»Fe-O)$_2$-SeO_3^{4-}, (»Fe-OH_2)$_2$-SeO_3
27	»Fe-OH-SeO_3^{2-}, »Fe-OH_2-$HSeO_3$, (»Fe-O)$_2$-SeO_3^{4-}	**60**	»Fe-OH-SeO_3^{2-}, »Fe-OH_2-SeO_3^-, »Fe-OH_2-$SeO_3H_2^+$, (»Fe-O)$_2$-SeO_3^{4-}, (»Fe-OH_2)$_2$-SeO_3
28	»Fe-OH-SeO_3^{2-}, »Fe-OH_2-$HSeO_3$, (»Fe-OH_2)$_2$-SeO_3	**61**	»Fe-OH-SeO_3^{2-}, »Fe-OH_2-$HSeO_3$, »Fe-OH_2-$SeO_3H_2^+$, (»Fe-O)$_2$-SeO_3^{4-}, (»Fe-OH_2)$_2$-SeO_3
29	»Fe-OH-SeO_3^{2-}, »Fe-OH_2-$SeO_3H_2^+$, (»Fe-O)$_2$-SeO_3^{4-}	**62**	»Fe-OH_2-SeO_3^-, »Fe-OH_2-$HSeO_3$, »Fe-OH_2-$SeO_3H_2^+$, (»Fe-O)$_2$-SeO_3^{4-}, (»Fe-OH_2)$_2$-SeO_3
30	»Fe-OH-SeO_3^{2-}, »Fe-OH_2-$SeO_3H_2^+$, (»Fe-OH_2)$_2$-SeO_3		**Six species reaction**
31	»Fe-OH-SeO_3^{2-}, (»Fe-O)$_2$-SeO_3^{4-}, (»Fe-OH_2)$_2$-SeO_3	**63**	»Fe-OH-SeO_3^{2-}, »Fe-OH_2-SeO_3^-, »Fe-OH_2-$HSeO_3$, »Fe-OH_2-$SeO_3H_2^+$, (»Fe-O)$_2$-SeO_3^{4-}, (»Fe-OH_2)$_2$-SeO_3
32	»Fe-OH_2-SeO_3^-, »Fe-OH_2-$HSeO_3$, »Fe-OH_2-$SeO_3H_2^+$		

The simulation results showed that only ten combinations, out of 63, can effectively simulate the Se(IV) sorption data (Table 5). A good quality model had not been obtained when four, five, and six surface complexation reactions were used. In addition, the contribution of surface species to model quality was observed: »Fe-OH-SeO_3^{2-} species are always included in the good quality models and despite the introduction of additional species other than »Fe-OH-SeO_3^{2-} species, the R value was only slightly improved. In other words, even though a number of surface complexation reactions had been reported in the literature, full community sorption data can be effectively fitted using only one species, i.e. »Fe-OH-SeO_3^{2-}, and only nominal increases in R are achieved with the

addition of multiple surface species. Figure 5 describes the simulation results obtained from the best quality SCM construct. As shown in the graphs, surface complexation reaction constants produced by the community data-driven workflow can reproduce most of the experimental data effectively.

Table 5. Surface complexation models with good quality fit

Number of reactions	Surface species	R value
1	»Fe-OH-SeO_3^{2-}	0.9131
2	»Fe-OH-SeO_3^{2-}, »Fe-OH_2-SeO_3^-	0.9192
2	»Fe-OH-SeO_3^{2-}, »Fe-OH_2-$HSeO_3$	0.9202
2	»Fe-OH-SeO_3^{2-}, »Fe-OH_2-$SeO_3H_2^+$	0.9198
2	»Fe-OH-SeO_3^{2-}, (»Fe-O)$_2$-SeO_3^{4-}	0.9002
2	»Fe-OH-SeO_3^{2-}, (»Fe-OH_2)$_2$-SeO_3	0.9204
3	»Fe-OH-SeO_3^{2-}, »Fe-OH_2-SeO_3^-, (»Fe-O)$_2$-SeO_3^{4-}	0.9083
3	»Fe-OH-SeO_3^{2-}, »Fe-OH_2-$HSeO_3$, (»Fe-O)$_2$-SeO_3^{4-}	0.9085
3	»Fe-OH-SeO_3^{2-}, »Fe-OH_2-$SeO_3H_2^+$, (»Fe-O)$_2$-SeO_3^{4-}	0.9111
3	»Fe-OH-SeO_3^{2-}, »Fe-OH_2-$SeO_3H_2^+$, (»Fe-OH_2)$_2$-SeO_3	0.9206

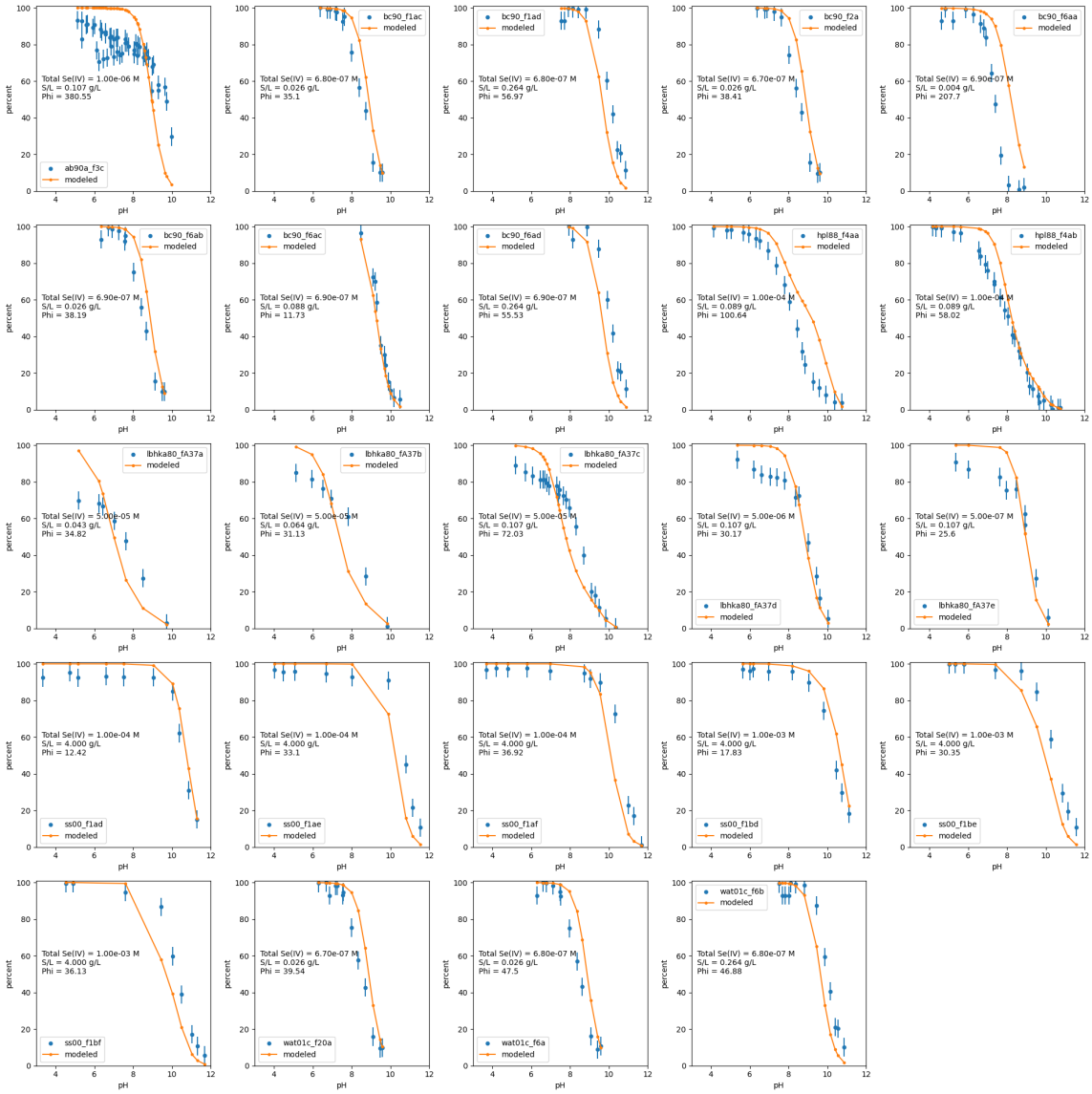

Figure 5. Simulation results for Se(IV) sorption to ferrihydrite obtained from the best SCM cosntuct. Datapoints colored in blue represent experimental data and orange solid lines represent modeled data from L-ASCM.

Simulation results showed that community data-driven surface complexation modeling approach also can describe sorption features across multiple oxidation states that are internally consistent. For example, it is widely known that sorption affinity of Se(IV) is higher than that of Se(VI). Using our approach and as shown in Table 6, surface complexation reaction constant obtained for Se(IV) are greater than Se(VI) when the reactions have the same reaction stoichiometry.

Table 6. One species surface complexation model for Se(IV) and Se(VI) sorption to ferrihydrite

Surface Complexation Reaction	Se(IV)	Se(VI)
»Fe-OH + $SeO_{3(4)}^{2-}$ ↔ »Fe-OH-$SeO_{3(4)}^{2-}$	6.33 ± 0.04	1.08 ± 0.04

3.3 Outlook and Future Work

The model developed through the present task showed its ability for automation of simulation workflow for modeling sorption phenomena. Therefore, it was made possible to examine a lot of SCM constructs for obtaining the best quality model which can reproduce experimental data. Follow up studies have been conducted to analyze the sorption phenomena of selenium to various iron oxides. Since the developed framework is readily expandable (as community data increase) and extensible (as the number of minerals increase), the framework can be easily applied to other sorption system of interest. We will complete our analysis of Se(IV) and Se(VI) sorption to ferrihydrite, goethite, hematite, magnetite, and maghemite in FY23 and plan to submit a manuscript summarizing these results in early FY24.

4. FY24 Planned Efforts

Observed changes in radionuclide adsorption after bentonite/clay heating have implications for radionuclide diffusive transport through engineered barriers and must be considered when designing waste disposal repositories. Sorption experiments and data analysis for ^{137}Cs and for ^{243}Am will be completed by the end of FY23. In FY24, we will complete the study including all other radionuclides reported in Table 1 and perform a modeling analysis to identify processes and mechanisms driving the observed changes in radionuclide sorption behavior. Results from our comprehensive analysis will inform performance assessment models on how much reduction in Kd values can be expected for the original clay material as a result of heating and interaction with near-field repository materials (e.g. steel, concrete, granite).

Our FY22 effort focused on completing our analysis of radionuclide incorporation into Fe oxide phases and evaluation of λ_{Me} values across a range of radionuclides relevant to performance assessment models and demonstrating our approach using Se as an example. In FY24, we will submit a manuscript detailing our analysis of Se adsorption and incorporation into iron oxide phases and summarize our mechanistic understanding of the relationship between adsorption and coprecipitation processes and how the relationship can be described numerically for modeling purposes.

Our analysis of Se surface complexation to iron oxide phases is now explicitly accounting for surface titration behavior of oxide surfaces that was the subject of a recently published manuscript (Han et al., 2023). With this in mind, our Se sorption analysis is yielding a more robust workflow for developing self-consistent surface complexation modeling approaches that can be adapted to specific SCM conceptual and numerical approaches (i.e. non-electrostatic, diffuse layer, triple layer models). In FY24,

we will publish the results of our comprehensive surface complexation modeling of Se(IV) and Se(VI) sorption to iron oxide mineral phases.

5. Acknowledgments

This work was supported by the Spent Fuel and Waste Science and Technology campaign of the Department of Energy's Nuclear Energy Program. Prepared by LLNL under Contract DE-AC52-07NA27344.

6. References

Benjamin, M.M., Bloom, N.S., 1981. Effects of Strong Binding of Anionic Adsorbates on Adsorption of Trace Metals on Amorphous Iron Oxyhydroxide, in: Tewari, P.H. (Ed.) Adsorption From Aqueous Solutions. Springer US, Boston, MA, pp. 41-60. doi.org/10.1007/978-1-4613-3264-0_3.

Brendler, V., Vahle, A., Arnold, T., Bernhard, G., Fanghänel, T., 2003. RES3T-Rossendorf expert system for surface and sorption thermodynamics. J Contam Hydrol 61(1-4), 281-291. doi.org/10.1016/s0169-7722(02)00129-8.

Caporuscio, F.A., Cheshire, M. C., Palaich, S., Norskog, K., Jove Colon, C. , 2015. Argillite Disposal R&D-LANL 2015. Summary of baseline experiments for generic repository engineered barriers. (FY 2015). (FCRD-UFD-2015-000356, LA-UR-15-26110). Los Alamos National Lab. (LANL), Los Alamos, NM (United States).

Caporuscio, F.A., Cheshire, M. C., Rearick, M. S., Jove Colon, C. , 2014. LANL argilliteEBS experimental program 2014. (FCRD-USED-2014-000491). Los Alamos National Lab. (LANL), Los Alamos, NM (United States).

Caporuscio, F.A., Migdissov, A., Rock, M. J., Sauer, K. B., van Hartesveldt, N. F. , 2019. Engineered Barrier System R&D and International Collaborations–LANL (FY19) (No. LA-UR-19-24222). Los Alamos National Lab. (LANL), Los Alamos, NM (United States).

Caporuscio, F.A., Sauer, K.B., Rock, M.J., 2020. Engineered System R&D and International Collaborations – Los Alamos National Laboratory (FY18). SF&WD R&D Work package # SF-02LA01030801 Rev2/SF-20LA01030805, LA-UR-20-25330.

Caporuscio, F.A., Sauer, K.B., Rock, M.J., Houser, L.M., 2018. Engineered System R&D and International Collaborations – Los Alamos National Laboratory SF&WD R&D Work package # SF18LA01030801/SF-18LA01030805, LA-UR-18- 27601.

Cheshire, M.C., Caporuscio, F.A., Rearick, M.S., Jove-Colon, C., McCarney, M.K., 2014. Bentonite evolution at elevated pressures and temperatures: An experimental study for generic nuclear repository designs. American Mineralogist 99(8-9), 1662-1675.

Cuadros, J., Linares, J., 1996. Experimental kinetic study of the smectite-to-illite transformation. Geochimica Et Cosmochimica Acta 60(3), 439-453. doi.org/Doi 10.1016/0016-7037(95)00407-6.

Doherty, J., 2018. PEST: Model-Independent Parameter Estimation. Watermark Numerical Computing.

Dresden-Rossendorf, H.-Z., 2013. RES³T - Rossendorf Expert System for Surface and Sorption Thermodynamics. https://www.hzdr.de/db/RES3T.disclaimer. 2013).

Dzombak, D.A., Morel, F.M.M., 1990. Surface complexation modeling: hydrous ferric oxide. John Wiley & Sons.

Han, S.-C., Chang, E., Zechel, S., Bok, F., Zavarin, M., 2023. Application of community data to surface complexation modeling framework development: Iron oxide protolysis. J Colloid Interf Sci 648, 1015-1024. doi.org/https://doi.org/10.1016/j.jcis.2023.06.054.

Meunier, A., Velde, B., Griffault, L., 1998. The reactivity of bentonites: a review. An application to clay barrier stability for nuclear waste storage. Clay Minerals 33(2), 187-196. doi.org/10.1180/claymin.1998.033.2.01.

Mills, M.M., Sanchez, A.C., Boisvert, L., Payne, C.B., Ho, T.A., Wang, Y.F., 2023. Understanding smectite to illite transformation at elevated (>100 degrees C) temperature: Effects of liquid/solid ratio, interlayer cation, solution chemistry and reaction time. Chemical Geology 615. doi.org/ARTN 121214
10.1016/j.chemgeo.2022.121214.

Parkhurst, D.L., Appelo, C.A.J., 2013. Description of input and examples for PHREEQC version 3—A computer program for speciation, batch-reaction, one-dimensional transport, and inverse geochemical calculations, US geological survey techniques and methods. p. 497.

Pusch, R., 1979. Highly Compacted Sodium Bentonite for Isolating Rock-Deposited Radioactive-Waste Products. Nucl Technol 45(2), 153-157. doi.org/Doi 10.13182/Nt79-A32305.

Wang, P., Anderko, A., Turner, D.R., 2001. Thermodynamic modeling of the adsorption of radionuclides on selected minerals. II: Anions. Industrial and Engineering Chemistry Research 40(20), 4444-4455. doi.org/10.1021/ie000992h.

Wersin, P., Johnson, L.H., McKinley, I.G., 2007. Performance of the bentonite barrier at temperatures beyond 100 degrees C: A critical review. Physics and Chemistry of the Earth 32(8-14), 780-788. doi.org/10.1016/j.pce.2006.02.051.

Zavarin, M., Chang, E., Wainwright, H., Parham, N., Kaukuntla, R., Zouabe, J., Deinhart, A., Genetti, V., Shipman, S., Bok, F., Brendler, V., 2022. Community Data Mining Approach for Surface Complexation Database Development. Environ Sci Technol 56(4), 2827-2838. doi.org/10.1021/acs.est.1c07109.

Zheng, L., Rutqvist, J., Xu, H., Birkholzer, J.T., 2017. Coupled THMC models for bentonite in an argillite repository for nuclear waste: Illitization and its effect on swelling stress under high temperature. Eng Geol 230, 118-129. doi.org/10.1016/j.enggeo.2017.10.002.